*Original paper*

# Effect of active environment on the orientational organization of rod-like nanoparticle: mesoscale simulations

A.E. Virskiy[1], M.D. Malyshev[1], P.V. Komarov[2]
[1]*Tver State University, 170100, Tver, Russia*
[2]*Institute of Organoelement Compounds RAS, 119991, Moscow, Russia*
*aevirskiy@gmail.com*

DOI: 10.26456/pcascnn/2026.18.380

**Abstract:** This work examines the possibility of controlling the spatial orientation of rod-like nanoparticle through the influence of molecules of active environment. We consider ordered layers formed by smectic molecules to be an example of an active environment. To simulate the supramolecular organization in such conditions, we employed the dissipative particle dynamics method. Our result shows that when the nanoparticle length is twice the length of a molecule of the active environment, three types of orientational ordering are possible: localization inside a domain formed by the head groups of molecules of active environment (type I), inside a domain formed by the tail groups of molecules of the active environment (type II), and perpendicular to the domains of active environment (type III). The first two orientations are stable, while the orientation perpendicular domains is unstable for long simulation times. This may indicate the potential instability of such states. We also studied the influence of the nanoparticle length and the presence of residual solvent on the stability of the identified orientational orderings of the considered nanosystems. These results could be useful for developing liquid crystal materials reinforced with rod-like nanoparticles or a switchable nanoparticles orientation.

*Keyword: self-assembly, dissipative particle dynamics, nanoparticles, active environment.*

*Alexander E. Virskiy – 2nd year student, Tver State University, ORCID: 0009-0007-3139-8241*
*Maxim D. Malyshev – Ph. D., Associate Professor of Physical Chemistry Department, Tver State University, ORCID: 0000-0002-2799-7512*
*Pavel V. Komarov – Dr. Sc., Docent, Leading Researcher, Laboratory of Physical Chemistry of Polymers, A.N. Nesmeyanov Institute of Organoelement Compounds of RAS, ORCID: 0000-0003-2138-5088*

УДК 544.032.12

*Оригинальная статья*

# Влияние активной среды на пространственную организацию стержнеобразной наночастицы: мезомасштабное моделирование

А.Е. Вирский[1], М.Д. Малышев[1], П.В. Комаров[2]
[1]*ФГБОУ ВО «Тверской государственный университет»*
*170002, Россия, Тверская область, Тверь, Садовый пер.,35*
[2]*ФГБУН «Институт элементоорганичесих соединений им. А.Н. Несмеянова РАН»*
*119991, Россия, Москва, ул. Вавилова, 28*
*aevirskiy@gmail.com*

DOI: 10.26456/pcascnn/2026.18.380

**Аннотация:** В данной работе рассматривается возможность управления пространственной ориентацией стержнеобразной наночастицы посредством воздействия на неё молекулами активной среды. В качестве активной среды мы рассматриваем упорядоченные слои, формируемые молекулами смектиков. Для моделирования супрамолекулярной организации в таких средах мы задействовали метод диссипативной динамики частиц. Результаты нашего исследования показывают, что при длине наночастицы, в два раза превышающей длину молекулы активной среды, возможны три типа ориентационных упорядочений: локализация

© A.E. Virskiy, M.D. Malyshev, P.V. Komarov, 2026

внутри домена, формируемого головной частью молекул активной среды (тип I), внутри домена, образованного хвостовой частью молекул активной среды (тип II), и перпендикулярно доменам активной среды (тип III). Первые две ориентации являются стабильными, в то время как ориентация поперек доменов неустойчива на больших временах в нашем моделировании. Это может свидетельствовать о потенциальной неустойчивости таких состояний. Также изучено влияние длины наночастицы и наличие остаточного растворителя на стабильность выявленных ориентационных упорядочений, рассмотренных наносистем. Полученные результаты могут быть полезны для разработки жидкокристаллических материалов, армированных стержнеобразными наночастицами, или с переключаемой ориентацией наночастиц.

*Ключевые слова: самосборка, диссипативная динамика частиц, наночастицы, активная среда.*

*Вирский Александр Евгеньевич – студент 2 курса физико-технического факультета ФГБОУ ВО «Тверской государственный университет»*
*Малышев Максим Дмитриевич – к.ф.-м.н., доцент кафедры физической химии ФГБОУ ВО «Тверской государственный университет»*
*Комаров Павел Вячеславович – д.ф.-м.н., доцент, ведущий научный сотрудник лаборатории физической химии полимеров ФГБУН «Институт элементоорганических соединений им. А.Н. Несмеянова РАН»*

Поступила в редакцию/received: 17.07.2026; после рецензирования/revised: 25.08.2026; принята/accepted 30.08.2026.

## 1. Introduction

The self-assembly process is currently considered a promising basis for modern technology in obtaining nanomaterials with specific structures through the spontaneous ordering of molecular building blocks. Using this process, researchers have already obtained supramolecular self-assembled monolayers, nanocapsules for controlled drug delivery, photonic crystals, metal-organic frameworks, and many other structures [1-4]. The shape of the molecular building blocks, the nature of the intermolecular interactions, and the environmental parameters can act as control factors for self-assembly. For instance, melts of AB diblock copolymers can form domains with different symmetries depending on the block length ratio and thermodynamic compatibility [5]. Complex organic mesogens with anisotropic shapes, such as cholesterol derivatives – cyclic lipophilic alcohols – also have the ability to self-assemble [6]. Their spatial structures resemble small, flat bars or rigid rods with polar heads and nonpolar tails. These molecules can form various mesophases, i.e., liquid crystalline states.

Nanoparticles (NPs) are commonly used to modify the properties of nanomaterials. They can change the mechanical, electrical, and thermal properties of a host phase [7-9]. The host phase is the dominant molecular subsystem that includes NPs as constituent units of the emerging structure. However, due to their high surface energy, NPs can form large, disordered aggregates. Increasing their weight fraction can negatively affect the mechanical properties of nanosystems [10]. Therefore, it is important to find ways to control the spatial ordering of NPs. The ability of host phase molecules to form ordered domains can be used as a controlling factor. When they selectively interact with

the host phase, the latter acts as an active environment that can control the spatial ordering of the NPs. For example, [11] showed that the selective interaction with diblock copolymer domains allows for the control of the spatial localization of spherical gold NPs. An increase in their concentration provokes the transformation of the lamellar phase into a distorted hexagonal phase.

If NPs are anisotropic, i.e., rod-like or flat, and their dimensions are comparable to the period of the host phase domains, it becomes possible to control their spatial orientation. Examples of rod-like NPs include single-walled and multi-walled carbon nanotubes, metallic nanorods, and nanowires. Embedding them into a smectic host can improve the material's mechanical and electro-optical properties [12]. Flat NPs include clays, graphene, and boron nitride NPs. These particles are also used to enhance the mechanical properties of polymers [10]. Very few studies are devoted directly to controlling the spatial orientation of anisotropic NPs. In the case of two-dimensional (2D) NPs, this issue was examined in detail in [13], where the interaction between diblock copolymer domains and a flat NP was investigated. The study showed that, in the regime of strong segregation of symmetric copolymer blocks, NPs can be embedded in one of the domains or located perpendicular to them when lamellar domains arise in the system. Thus, the nanomaterial described in ref. [13] can be classified as a two-state nanocomposite, i.e., a material with two stable NP orientations. However, the literature contains few studies on controlling the orientation of a single rod-like NP (RNP) through an active environment. Among the works found, a few studies can be noted in which the hydrophobic interaction of the rods [14] and the electrostatic field [15] were used as controlling factors.

The aim of this work is to study the possibility of controlling the orientation of RNPs. We consider ordered layered structures formed by smectic molecules as an active environment. These structures' characteristic scale can range from 2 to 4 nm. In this case, the RNP size should be greater than or comparable to the period of the domains formed by MAE. Since we are interested in the possible self-organization in such systems, we use dissipative particle dynamics (DPD) as a modeling method [16]. DPD is a mesoscale method most often used to predict the supramolecular organization of soft matter [16, 17].

## 2. Model and modeling method

As mentioned in the introduction, we used the DPD method to investigate the raised question. The method represents molecules and NPs as sets of structureless particles with the same diameter, $\sigma = 1$. The evolution of the system is described using a system of Newtonian equations. The resultant force applied to the $i$-th bead is determined by the sum of the conservative (describing

interparticle interactions), dissipative and random forces (responsible for thermostatting the system). These forces enable us to approximate complex molecular structures.

The type of bead determines the nature of the intermolecular interaction, which is regulated by the maximum repulsion amplitude parameter of the conservative force $a_{ij}$, which is related to the Flory-Huggins parameters $a_{ij} \propto \chi_{ij}$. The latter is calculated using Hildebrand solubility parameters [18] $\delta_i$, where $\chi_{ij} \propto (\delta_i - \delta_j)^2$. Therefore, the smaller the difference in solubility parameters, the higher the affinity of the interacting beads and vice versa. Varying the $\delta_i$ parameters adjusts the compatibility of the model subsystems, which is equivalent to scanning the chemical space of possible compounds and the properties of the environment. By simplifying the molecular structure and using soft interaction potentials between beads, DPD becomes an effective tool for studying structural transitions in supramolecular systems. Now, let us describe the developed model.

Our model contains three subsystems (see fig. 1 a): a rod-like NP made of $N$ beads of type A; a molecule of the active environment consisting of two types of beads, B and C, arranged in a head-tail structure; and beads corresponding to the solvent, D. Subsystem D was introduced to account for the influence of solvents and low-molecular substances that can enter the nanostructure during its preparation and use. This figure also illustrates the primary parameters of the molecular objects, including the stiffness parameter of bond deformation potential, the equilibrium bond length of the NP and MAE ($K_b$ = 200, $l$ = 1), and the deformation potential of the angle between the beads and their equilibrium values for the NP and MAE ($K_{a,NP}$ = 25, $\theta_{NP}$ = 180°, $K_{a,MAE}$, $\theta_{MAE}$ = 180°). The values of $K_{a,NP}$ and $\theta_{NP}$ ensure that the NP maintains its rod-like conformation. From this point forward, the model parameter values are given in dimensionless DPD units. The value of $\theta_{MAE}$ was chosen to be equal to $\theta_{NP}$, and $K_{a,MAE}$ was chosen during test calculations (see the next section).

Given the size of the smectic molecules and the chosen representation of the active environmental molecule, 0,8 nm is a convenient unit of scale, $\sigma$. This value roughly corresponds to the smallest possible diameter of a single-walled carbon nanotube. In this case, the MAE can be constructed from three to five beads. The parameterization of intermolecular interactions was chosen based on the following considerations. Since smectic molecules contain polar groups ($-OH$, $-NO_2$, halogens, etc.) and subsystem D can be associated with water vapor, a maximum value of $\delta$ = 40,7 $(\text{MPa})^{1/2}$ was chosen, which corresponds to Hildebrand's solubility parameter for water. The minimum value of $\delta$ was set to 14 $(\text{MPa})^{1/2}$, corresponding to the hydrocarbon fragments in the smectic molecules.

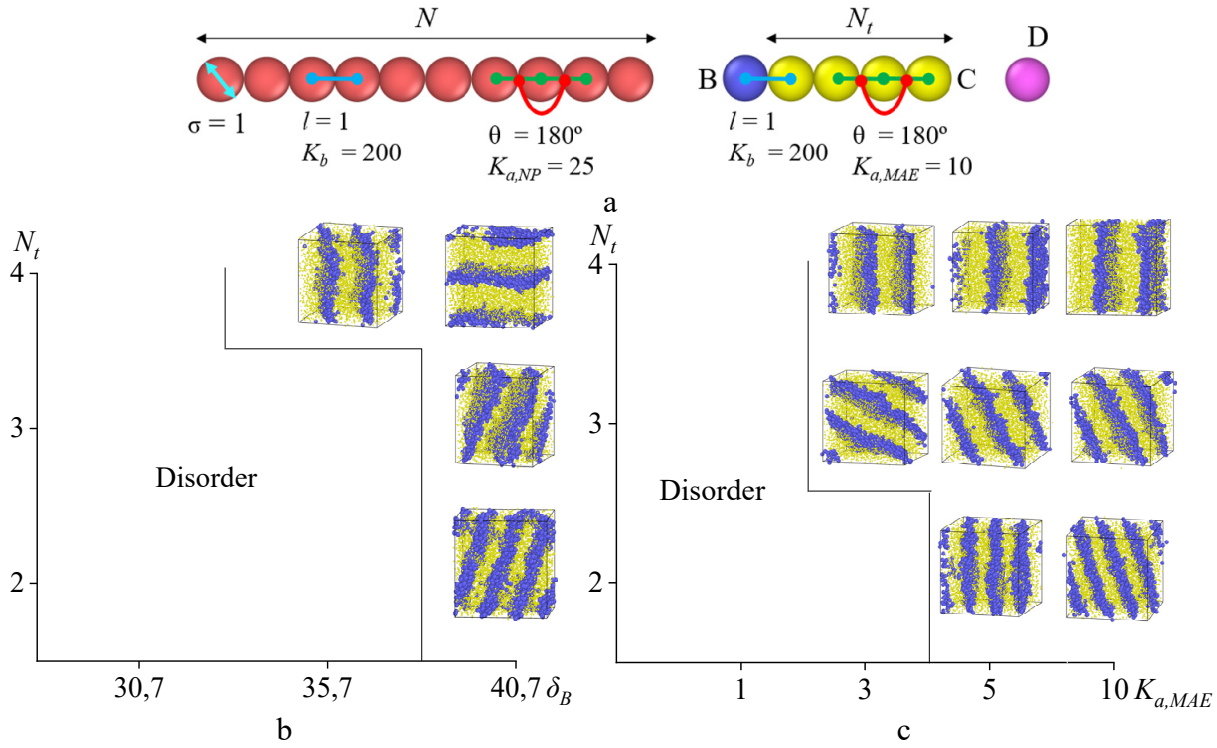


Fig. 1. The main components of the model and their prototypes (a). The letters correspond to the following: type A beads (NP fragments), type B and C beads (fragments of active environment molecules), and type D beads (solvent). The model parameterization is shown separately. $K_b$ and $K_a$ are the bond strain stiffness potential parameters and the angle between the bonds, respectively, while $l$ and $\theta$ are the equilibrium bond length and angle values, respectively. System state diagram in coordinates $N_t$ vs $\delta_B$ at fixed $K_{a,MAE} = 10$ (b); $N_t$ vs $K_{a,MAE}$ at fixed $\delta_B = 40{,}7$ (c).

## 3. Results

All calculations were performed using the LAMMPS software package [19] and the standard DPD method parameterization [16]. The simulated systems were placed in a cubic simulation cell with an edge length of 12-13 $\sigma$ and periodic boundary conditions. The initial configurations were prepared using our homemade software constructor as follows. First, NP was randomly generated in the simulation cell. Then, the remaining space was filled with MAE and solvent to ensure an average system number density of 3. Next, the systems were equilibrated in the athermal regime (all $a_{ij} = 25$) for 100,000 DPD steps. Finally, the interaction parameters were smoothly switched to the working values for 250,000 DPD steps. The final relaxation phase lasted 500,000 DPD steps until equilibrium was reached. To verify the stability of the obtained states, we used the «annealing» procedure, which involves smoothly varying the interaction parameters $a_{ij}$ for a selected pair of subsystems over time. To check the stability of these states, we used an «annealing» procedure involving smoothly varying the interaction parameters over time for selected pairs of

subsystems, as well as abruptly changing them (quenching) and allowing for relaxation afterwards.

In the first stage of the calculations, the parameters $\delta_B$, $\delta_C$, $K_a$, and $N_t$ were selected. Since subsystem C corresponded to the hydrocarbon fragment of MAE, $\delta_C = 14$ (MPa)$^{1/2}$. The value of $\delta_B$ varied from 14 to 47 (MPa)$^{1/2}$, and $N_t$ varied from 2 to 4. Fig. 1 b shows the state diagram in $N_t$ versus $\delta_B$ coordinates with a fixed $K_{a,MAE}$ value of 10. As can be seen in the figure, a well-defined lamellar ordering arises in the system when there is strong segregation between subsystems B and C, which is typical of smectics consisting of $-OH$ groups and hydrocarbon parts. When $\delta_B = 40{,}7$ (MPa)$^{1/2}$, the lamellar orders are stable throughout the range of $N_t$ variations. Note that, when $N_t = 4$ ($\sigma = 0{,}8$ nm), the coarse-grained model of MAE corresponds to a cholesterol molecule with $C_{27}H_{45}OH$. Therefore, $N_t = 4$ was chosen for subsequent calculations. To check the sensitivity of our model to changes in $K_{a,MAE}$ and $N_t$, we constructed a second state diagram in $N_t$ versus $K_{a,MAE}$ coordinates (see fig. 1 c). As can be seen in the figure, decreasing $N_t$ or weakening $K_{a,MAE}$ reduces the stability of the lamellar ordering of subsystems B and C. We chose the following set of parameters since we need stable microphase separation in the active medium for further calculations, namely $\delta_B = 40$ (MPa)$^{1/2}$, $\delta_C = 14$ (MPa)$^{1/2}$, $K_{a,MAE} = 10$, and $N_t = 4$.

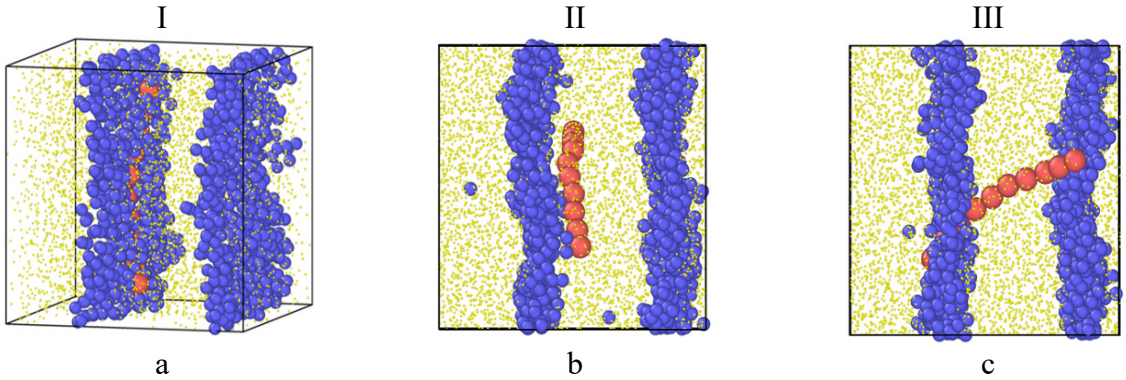


Fig. 2: Basic types of spatial and orientational organization of NP stable states: a – $a_{AB} = a_{AC} = 25$ and $a_{AB} = a_{AC} = 50$, b – $a_{AB} = 50$ and $a_{AC} = 25$. The transitional state (c) occurs when the NP is partially compatible with one of the subsystems. Roman numerals are used for ease of designation. The color coding of the beads corresponds to fig. 1.

The second stage of calculations aimed to identify the primary spatial arrangements of NP's in relation to the MAE domains within the context of strong segregation of their head and tail components ($a_{BC} = 53$). The calculations were performed for $N = 10$, meaning the NP length was twice that of $N_t$.

Two stable and one unstable orientation of NP were identified (see fig. 2). The first orientation (see fig. 2 a) occurs when NP is fully compatible with one subsystem and incompatible with the other, corresponding to two sets of

parameters: $a_{AB}=a_{AC}=25$ and $a_{AB}=a_{AC}=50$. The second type of orientation (see fig. 2 b) corresponds to $a_{AB}=50$ and $a_{AC}=25$, meaning NP is compatible with subsystem C and incompatible with subsystem B. The third type of orientation (see fig. 2 c) is transitional between the first and second. This state usually arises with partial compatibility with one of the subsystems and is characterized by a spontaneous transition to one of the stable states, depending on the given set of parameters.

As mentioned earlier, the stability of the identified states was tested using annealing procedures in which the interaction parameters were periodically varied within a specified range. Fig. 3 shows the kinetics of transitions between states I, II, and III over five cycles of annealing. The system transitioned between states I and II with a fixed $a_{AB}$ value of 50 while the $a_{AC}$ value was periodically changed from 50 to 25 and back to 50. State III arose spontaneously and could be maintained by repeating cyclic changes in $a_{AC}$. However, this state was not stable on its own. When NP adopted state III, relaxation with $a_{AC}=25$ or 50 caused it to spontaneously return to state I (with $a_{AC}=50$) or state II (with $a_{AB}=25$). This was due to the energy gained from the reduction in the number of contacts between the NP and the B-beads subsystem.

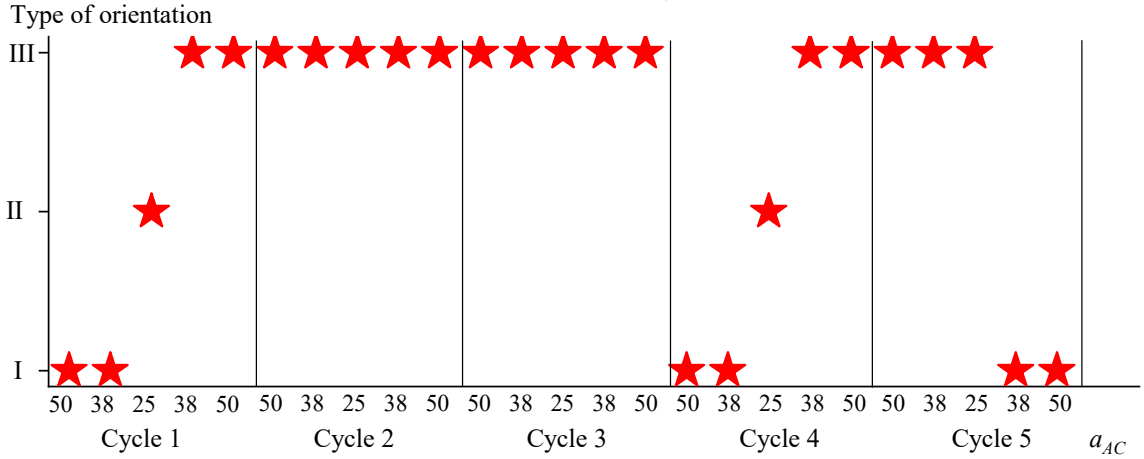


Fig. 3. An example of the transitions between the main spatial and orientation orderings of the NP, depending on changes in the interaction parameter $a_{AC}$.

Fig. 4 shows all possible orientational transitions of NP when it is incompatible with MAE in the initial state. Transition number 1 represents the process of preparing the initial configuration of the system, as described above. During this process, NP integrates with subsystem B in state I. It is important to note that when the parameters and $a_{AC}$ are set to 50, NP remains localized in subsystem B during both smooth transitions and abrupt switches from the athermal state to $a_{AB}=a_{AC}=50$.

Process 2, the transition from orientation I to II, can be achieved by smoothly changing the $a_{AC}$ parameter from 50 to 25 or by abruptly switching

between these values. However, if $a_{AC}$ reaches 38, an I to III transition may spontaneously occur instead of the I to II transition. Note that the system may remain in state III when $a_{AC}$ is 25 or 50 for an extended period. After prolonged relaxation the NP will always spontaneously transition from state III to state II.

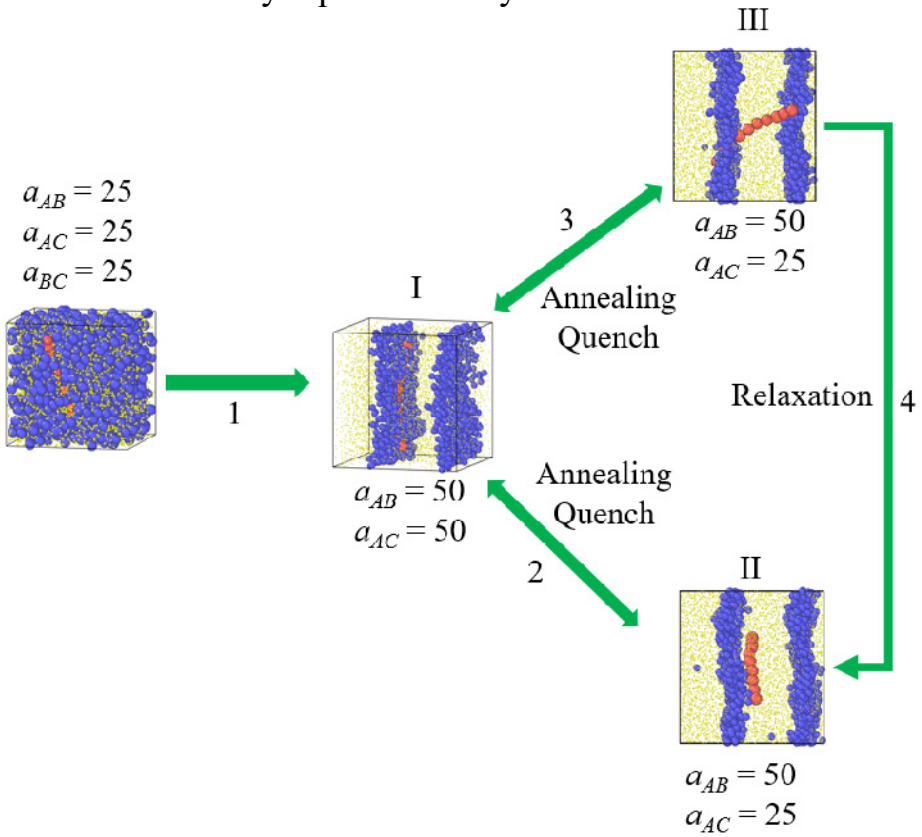


Fig. 4. Identified Orientational Transitions of NP's for $N = 10$ (Numbers 1 – 4). Arrows indicate transition directions. The color coding corresponds to that in fig. 1. Roman numerals correspond to the main orientational orderings of NP's (see fig. 2).

Similar orientational transitions are also possible from state I, which arises when $a_{AB} = a_{AC} = 25$. In this case, the control parameter is $a_{AB}$ (changing from 25 to 50). To verify the influence of $N$ on the stability of the identified spatial ordering of NPs, we performed a series of simulations for $4 \leq N \leq 12$. Our results show that, as $N$ decreases, the mobility of the NPs increases. This leads to shorter residence times in state III. This explains the quasi-stable nature of state III for $N = 10$ due to the steric effect of parallelly ordered molecules in the active environment. The transition between states III and II deforms the rod-like conformation of MAE, requiring additional work. The system can draw energy from fluctuations in NP kinetic energy to accomplish this process (process 4 in fig. 4), so less fluctuation energy is needed for the transition as $N$ decreases.

To test the stability of the identified ordering at $N = 10$ one more time, a series of calculations was performed in the presence of a solvent (subsystem D). The case in which the solvent was compatible with all subsystems of the model was considered. Based on the results, the lamellar ordering of the MAE system

occurs when the residual solvent volume fraction is below 10%. All of the identified orientations were accurately reproduced (see fig. 5).

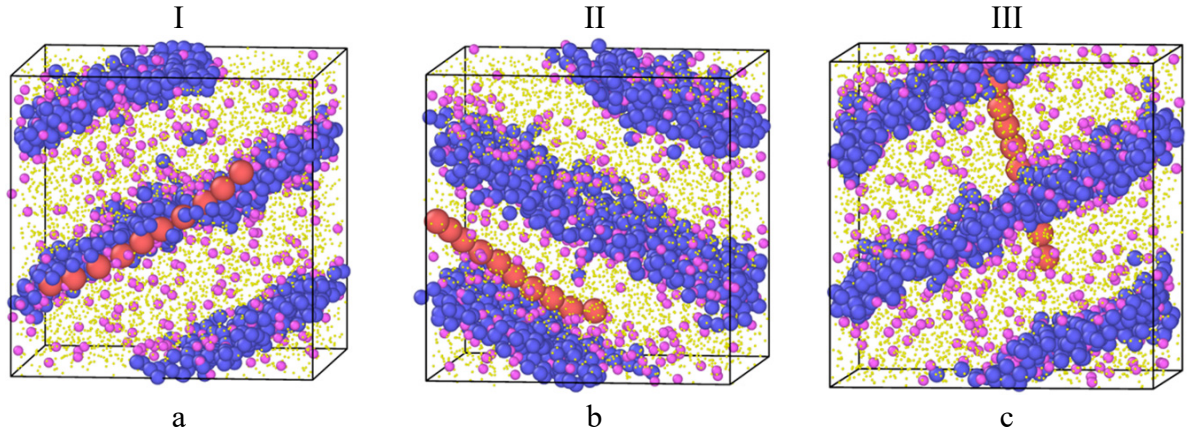


Fig. 5. Examples of the reproduction of NP orientational orderings (I-III) when a solvent is introduced into the system. The color coding corresponds to that in fig. 1.

## 4. Conclusion

We studied the possibility of controlling the spatial orientation of rod-like NPs under the influence of molecules in an active environment. Three types of orientational order for RNP were identified in our system in which the length of the NPs was twice that of the RNP molecules localized within domains formed by a molecule's head (type I); within domains formed by its tail (type II); and perpendicular to both domains (type III). Types I and II are stable with regard to variations in the interaction parameters, which simulates the influence of external factors, such as temperature. However, NP orientation across domains is unstable over long relaxation times. The effect of length and residual solvent on stability was also investigated. However, DPD may not correctly reproduce the dynamics of a real molecular system due to the introduction of coarsening of the structure of the studied molecular prototypes [20]. More accurate forecasts about the stability of the third orientational ordering can be made through independent verification by other modeling methods. This will be accomplished in our next research. Our results could be useful for creating liquid crystal orderings reinforced with rod-like NPs, such as single-walled carbon nanotubes.

The research was carried out using the equipment of the shared research facilities of HPC computing resources at Lomonosov Moscow State University [21].

*P.V. Komarov acknowledges support from the Ministry of Science and Higher Education of the Russian Federation (contract no. 075-03-2026-024).*

**References:**

1. Singh M., Kaur N., Comini E. The role of self assembled monolayers in electronic devices, *Journal of Materials Chemistry C*, 2020, vol. 8, issue 12, pp. 3938-3955, DOI: 10.1039/D0TC00388C.
2. Weiden J., Bastings M.M.C. DNA origami nanostructures for controlled therapeutic drug delivery, *Current*

*Opinion in Colloid & Interface Science*, 2021, vol. 52, art. no. 101411, 14 p. DOI: 10.1016/j.cocis.2020.101411.
3. Mizeikis V., Juodkazis S., Marcinkevicius A. et al. Tailoring and characterization of photonic crystals, *Journal of Photochemistry and Photobiology C: Photochemistry Reviews*, 2001, vol. 2, issue 1, pp. 35-69, DOI: 10.1016/S1389-5567(01)00009-0.
4. Burnett B.J., Choe W. Sequential self assembly in metal–organic frameworks, *Dalton Transactions*, 2012, vol. 41, issue 13, pp. 3889-3894, DOI: 10.1039/C2DT12103D.
5. Khalatur P.G., Khokhlov A.R. Nonconventional scenarios of polymer self assembly, *Soft Matter*, 2013, vol. 9, issue 45, art. no. 10943, 12 p. DOI: 10.1039/c3sm52181h.
6. Kato T. Self assembly of phase segregated liquid crystal structures, *Science*, 2002, vol. 295, issue 5564, pp. 2414-2418, DOI: 10.1126/science.1070967 a.
7. Ondreas F., Lepcio P., Zboncak M. et al. Effect of nanoparticle organization on molecular mobility and mechanical properties of polymer nanocomposites, *Macromolecules*, 2019, vol. 52, issue 16, pp. 6250-6259, DOI: 10.1021/acs.macromol.9b01197.
8. Coetzee D., Venkataraman M., Militky J., Petru M. Influence of nanoparticles on thermal and electrical conductivity of composites, *Polymers*, 2020, vol. 12, issue 4, art. no. 742, 25 p. DOI: 10.3390/polym12040742.
9. Chen J., Yan L. Effect of carbon nanotube aspect ratio on the thermal and electrical properties of epoxy nanocomposites, *Fullerenes, Nanotubes and Carbon Nanostructures*, 2018, vol. 26, issue 11, pp. 793-800. DOI: 10.1080/1536383X.2018.1476345.
10. Wu Q., Miao W.S., Zhang Y.D. et al. Mechanical properties of nanomaterials: a review, *Nanotechnology Reviews*, 2020, vol. 9, issue 1, pp. 259-273, DOI: 10.1515/ntrev 2020 0021.
11. Sides S.W., Kim B.J., Kramer E.J., Fredrickson G.H. Hybrid particle field simulations of polymer nanocomposites, *Physical Review Letters*, 2006, vol. 96, issue 25, pp. 250601-1-250601-4. DOI: 10.1103/PhysRevLett.96.250601.
12. Bukowczan A., Hebda E., Pielichowski K. The influence of nanoparticles on phase formation and stability of liquid crystals and liquid crystalline polymers, *Journal of Molecular Liquids*, 2020, vol. 322, art. no. 114849, 31 p. DOI: 10.1016/j.molliq.2020.114849.
13. Malyshev M., Guseva D., Komarov P. Two state nanocomposite based on symmetric diblock copolymer and planar nanoparticles: Mesoscopic simulation, *Molecular Systems Design & Engineering*, 2024, vol. 9, issue 5, pp. 409-422, DOI: 10.1039/D3ME00176H.
14. Cheng C.C., Liu M.H., Mou C.Y., Chen Y.F. Controllable orientation of assembled gold nanorods on unstructured substrates, *RSC Advances*, 2013, vol. 3, issue 40, pp. 17696-17699, DOI: 10.1039/c3ra41357h.
15. Smith P.A., Nordquist C.D., Jackson et al. Electric field assisted assembly and alignment of metallic nanowires, *Applied Physics Letters*, 2000, vol. 77, issue 9, pp. 1399-1401. DOI: 10.1063/1.1290272.
16. Español P., Warren P.B. Perspective: dissipative particle dynamics, *Journal of Chemical Physics*, 2017, vol. 146, issue 15, pp. 150901-1-150901-16, DOI: 10.1063/1.4979514.
17. Komarov, P.V., Malyshev, M.D., Baburkin, P.O. Mesoscale modeling of solvent evaporation from the surface of a jet of spinning solution of polyacrylonitrile in dimethyl sulfoxide, *Journal of Structural Chemistry*, 2025, vol. 66, issue 12, pp. 2674-2683, DOI: 10.1134/s0022476625120194.
18. Hildebrand, J.H., Scott, R.L. *The solubility of nonelectrolytes*. New York: Reinhold Publishing, 1950, 488 p.
19. Thompson A.P., Aktulga H.M., Berger R. et al. LAMMPS – a flexible simulation tool for particle based materials modeling at the atomic, meso, and continuum scales, *Computer Physics Communications*, 2022, vol. 271, art. no. 108171, 34 p. DOI: 10.1016/j.cpc.2021.108171.
20. Rudzinski J.F. Recent progress towards chemically specific coarse grained simulation models with consistent dynamical properties, *Computation*, 2019, vol. 7, issue 3, art. no. 42, 28 p. DOI: 10.3390/computation7030042.
21. Voevodin Vl., Antonov A., Nikitenko D. et. al. Supercomputer Lomonosov-2: large scale, deep monitoring and fine analytics for the user community, *Supercomputing Frontiers and Innovations*, 2019, vol. 6, issue 2, pp. 4-11. DOI: 10.14529/jsfi190201.

**Библиографический список:**

1. **Singh, M.** The role of self assembled monolayers in electronic devices / M. Singh, N. Kaur, E. Comini // Journal of Materials Chemistry C. – 2020. – V. 8. – I. 12. – P. 3938-3955. DOI: 10.1039/D0TC00388C.
2. **Weiden, J.** DNA origami nanostructures for controlled therapeutic drug delivery / J. Weiden, M.M.C. Bastings / Current Opinion in Colloid & Interface Science. – 2021. – V. 52. – Art. № 101411. – 14 p. DOI: 10.1016/j.cocis.2020.101411.
3. **Mizeikis, V.** Tailoring and characterization of photonic crystals / V. Mizeikis, S. Juodkazis, A. Marcinkevicius et al. // Journal of Photochemistry and Photobiology C: Photochemistry Reviews. – 2001. – V. 2. – I. 1. – P. 35-69. DOI: 10.1016/S1389-5567(01)00009-0.

4. **Burnett, B.J.** Sequential self assembly in metal–organic frameworks / B.J. Burnett, W. Choe // Dalton Transactions. – 2012. – V. 41. – I. 13. – P. 3889-3894. DOI: 10.1039/C2DT12103D.
5. **Khalatur, P.G.** Nonconventional scenarios of polymer self assembly / P.G. Khalatur, A.R. Khokhlov // Soft Matter. – 2013. – V. 9. – I. 45. – Art. № 10943. – 12 p. DOI: 10.1039/c3sm52181h.
6. **Kato, T.** Self assembly of phase segregated liquid crystal structures / T. Kato // Science. – 2002. – V. 295. – I. 5564. – P. 2414-2418. DOI: 10.1126/science.1070967 a.
7. **Ondreas, F.** Effect of nanoparticle organization on molecular mobility and mechanical properties of polymer nanocomposites / F. Ondreas, P. Lepcio, M. Zboncak et al. // Macromolecules. – 2019. – V. 52. – I. 16. – P. 6250-6259. DOI: 10.1021/acs.macromol.9b01197.
8. **Coetzee, D.** Influence of nanoparticles on thermal and electrical conductivity of composites / D. Coetzee, M. Venkataraman, J. Militky, M. Petru // Polymers. – 2020. – V. 12. – I. 4. – Art. № 742. – 25 p. DOI: 10.3390/polym12040742.
9. **Chen, J.** Effect of carbon nanotube aspect ratio on the thermal and electrical properties of epoxy nanocomposites / J. Chen, L. Yan // Fullerenes, Nanotubes and Carbon Nanostructures. – 2018. – V. 26. – I. 11. – P. 793-800. DOI: 10.1080/1536383X.2018.1476345.
10. **Wu, Q.** Mechanical properties of nanomaterials: a review / Q. Wu, W.S. Miao, Y.D. Zhang et al. // Nanotechnology Reviews. – 2020. – V. 9. – I. 1. – P. 259-273. DOI: 10.1515/ntrev 2020 0021.
11. **Sides, S.W.** Hybrid particle field simulations of polymer nanocomposites / S.W. Sides, B.J. Kim, E.J. Kramer, G.H. Fredrickson // Physical Review Letters. – 2006. – V. 96. – I. 25. – P. 250601-1-250601-4. DOI: 10.1103/PhysRevLett.96.250601.
12. **Bukowczan, A.** The influence of nanoparticles on phase formation and stability of liquid crystals and liquid crystalline polymers / A. Bukowczan, E. Hebda, K. \Pielichowski // Journal of Molecular Liquids. – 2020. – V. 322. – Art. № 114849. – 31 p. DOI: 10.1016/j.molliq.2020.114849.
13. **Malyshev, M.** Two state nanocomposite based on symmetric diblock copolymer and planar nanoparticles: Mesoscopic simulation / M. Malyshev, D. Guseva, P. Komarov // Molecular Systems Design & Engineering. – 2024. – V. 9. – I. 5. – P. 409-422. DOI: 10.1039/D3ME00176H.
14. **Cheng, C.C.** Controllable orientation of assembled gold nanorods on unstructured substrates / C.C. Cheng, M.H. Liu, C.Y. Y.F. Chen // RSC Advances. – 2013. – V. 3. – I. 40. – P. 17696-17699. DOI: 10.1039/c3ra41357h.
15. **Smith, P.A.** Electric field assisted assembly and alignment of metallic nanowires / P.A. Smith, C.D. Nordquist, T.N. Jackson et al. // Applied Physics Letters. – 2000. – V. 77. – I. 9. – P. 1399-1401. DOI: 10.1063/1.1290272.
16. **Español, P.** Perspective: dissipative particle dynamics / P. Español, P.B. Warren // Journal of Chemical Physics. – 2017. – V. 146. – I. 15. – P. 150901-1-150901-16. DOI: 10.1063/1.4979514.
17. **Komarov, P.V.** Mesoscale modeling of solvent evaporation from the surface of a jet of spinning solution of polyacrylonitrile in dimethyl sulfoxide / P.V. Komarov, M.D. Malyshev, P.O. Baburkin // Journal of Structural Chemistry. – 2025. – V. 66. – I. 12. – P. 2674-2683. DOI: 10.1134/s0022476625120194.
18. **Hildebrand, J.H.** The solubility of nonelectrolytes / J.H. Hildebrand, R.L. Scott. – New York: Reinhold Publishing, 1950. – 488 p.
19. **Thompson, A.P.** LAMMPS – a flexible simulation tool for particle based materials modeling at the atomic, meso, and continuum scales / A.P. Thompson, H.M. Aktulga, R. Berger et al. // Computer Physics Communications. – 2022. – V. 271. – Art. № 108171. – 34 p. DOI: 10.1016/j.cpc.2021.108171.
20. **Rudzinski, J.F.** Recent progress towards chemically specific coarse grained simulation models with consistent dynamical properties / J.F. Rudzinski // Computation. – 2019. – V. 7. – I. 3. – Art. № 42. – 28 p. DOI: 10.3390/computation7030042.
21. **Voevodin, Vl.** Supercomputer Lomonosov-2: large scale, deep monitoring and fine analytics for the user Community / Vl. Voevodin, A. Antonov, D. Nikitenko et. al. // Supercomputing Frontiers and Innovations. – 2019. – V. 6. – I. 2. – P. 4-11. DOI: 10.14529/jsfi190201.